ChemPubSoc Europe

DOI: 10.1002/slct.201800714

Chemistry SELECT Full Papers

Sustainable Chemistry

Structural, Optical, Electrical and Electrocatalytic Activity Properties Of Luminescent Organic Carbon Quantum Dots

Ali Karatutlu,*[a, b] Bhushan Patil,[a, b] İsa Seker,[c] Sumeyra Istengir,[d] Atilla Bolat,[e] Osman Yildirim,[e] Yaşar N. Sevgen,[e] Yakup Bakış,[f] Bülend Ortaç,[a, b] Eda Yilmaz,[a, b] and Andrei Sapelkin[g]

Carbon is an essential element in human life and recently becoming technologically prominent due to the emerging field of "Carbononics". We demonstrate organic carbon quantum dots (qdots) containing nitrile bonded (C≡N bond) *d-glucose*-like traces in various sizes obtained from wheat flour to be promising for imaging applications and to possess a relaxor ferroelectric property and an enhanced electrocatalytic activity that could reduce the cost of energy devices and simple to scale up for the commercialization. The secondary electron microscopy (SEM) imaging shows that the particle size of carbon qdots can be controlled via the sonication exposure time. Elemental analysis and vibrational spectroscopy results show that carbon qdots are sensitive to N_2 gas in the atmosphere and could weaken its "carbogenic" property by making a stable C≡N bond at ambient atmosphere. Rietveld analysis and HR-TEM studies demonstrate that the structure of the C qdots was found to fit best with an acentric primitive orthorhombic lattice. The laser scanning confocal microscopy (LSCM) images show enhancement of the light emission when reducing the size and characteristic excitation wavelength-dependent light emission of C qdots. The photoluminescence and UV-Vis absorption spectroscopy techniques show surface dominant emission and absorption upon the nitrile bonding.

Introduction

Carbon (C) is known to be one of the fundamental blocks in human life and also becoming technologically important owing to recent structural discoveries such as CNTs[1,2] and Graphene.[3,4] Alternatively, C quantum dots (qdots) that are well-known semiconductor nanoparticles with sizes smaller than 100 nm seem to be promising for optical applications.[5,6] Furthermore, a wide range of synthesis methods has been applied for formation of stable C qdot to be used for catalytic oxidation activity.[7–9] Nevertheless, when toxicity of nanoparticles is concerned, the physicochemical behaviour[10–12] of qdots comes forth regardless of what it is made of. To minimise such issues, several green synthesis methods,[13–20] which require either heat, microwave or acoustic wave treatment, were chosen to form organic carbogenic qdots (referred as C qdots henceforth). One of the recent discoveries also shows that amorphous C qdots were found to be present within the *carbohydrate*-rich food products such as bread, sugar and jaggery[21] which may overcome such concerns at least for organic C qdots. From the elemental point of view, the authors consider wheat as a sustainable candidate for carbonization which can yield the formation of C qdots. Most vitally, wheat has a global importance for the food, the feed and the other industrial purposes. For instance, global wheat production in 2016/2017 season is forecast to be around 724 million tonnes by 1.4 percent decrease compared to 2015 record according to Food and Agriculture Organization (FAO) 2016 report.[22] Yet, international prices are expected to remain mostly stable. Wheat is also known to be one of the main vegetable protein sources within human food crops.[23] On the other hand, another issue is that cost-effective green synthesis methods were not available for the synthesis of organic C qdots at room temperature in mass scale without any chemical residual despite the fact that a possible synthesis mechanism from a carbohydrate source is available.[19] Therefore, it was attempted in this study to close this gap with wheat flour and bran for one pot green synthesis of luminescent C qdots in mass scale as an emerging qdot system[6] and discuss the possibility of

[a] *Dr. A. Karatutlu, Dr. B. Patil, Dr. B. Ortaç, Dr. E. Yilmaz*
UNAM-National Nanotechnology Research Center Bilkent University Ankara Turkey 06800
Tel: +903122903545
E-mail: ali@unam.bilkent.edu.tr
[b] *Dr. A. Karatutlu, Dr. B. Patil, Dr. B. Ortaç, Dr. E. Yilmaz*
The Institute of Materials Science and Nanotechnology Bilkent University Ankara Turkey 06800
[c] *Dr. İ. Seker*
Bio-Nanotechnology R & D Centre, Fatih University, Buyukcekmece, 34500, Istanbul, Turkey
[d] *S. Istengir*
Physics Department, Yildiz Technical University, 34220 Esenler, Istanbul, Turkey
[e] *A. Bolat, Prof. O. Yildirim, Dr. Y. N. Sevgen*
Electrical and Electronics Engineering, Arel University, 34295, Istanbul, Turkey
[f] *Dr. Y. Bakış*
Acarkent Doga IB World School, Acarkent Site, 3rd St, No:25, 34800 Acarkent, Beykoz, Istanbul, Turkey
[g] *Dr. A. Sapelkin*
Centre for Condensed Matter and Materials Physics, School of Physics and Astronomy, Queen Mary, University of London, E1 4NS,

Supporting information for this article is available on the WWW under https://doi.org/10.1002/slct.201800714

using such organic C qdots in imaging, electrical and catalytic applications. It is also shown in this study that the surface of C qdots can be stabilized with a nitrile bond upon exposing the sample to the ambient atmosphere or N_2 containing medium at room temperature. The method was found to be effective in the wheat flour as the size of the C qdots could be controllable. In order to understand ferroelectric characteristics of as-prepared C qdots, we simply come with an approach to have a temperature dependent electrical measurements as given for traditional ferroelectrics[24] to show that the C qdots might possibly represent a relaxor ferroelectric behaviour. Recent studies showed that the relaxor ferroelectrics due to the geometric frustrations could make ferroelectrics to be observed in a wide-ranging material types[25,26] despite the fact there are still some discussions[27] and objections[28] if such materials showing ferroelectric behaviour. We further proceed with an opportunity to utilize these samples in catalytic oxidation activity.

Results and Discussion

Optical Images and Structural Properties of C qdots

As a source material, we used both wheat flour and wheat bran as shown in Figure 1.

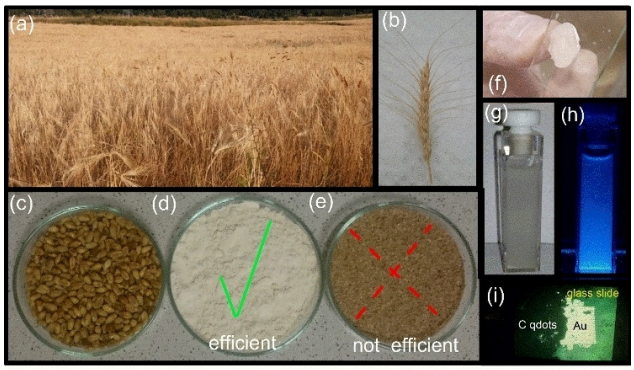

Figure 1. Optical Images (a) The images of a wheat field located in the Mediterranean region of Turkey, (b) a single wheat collected from this field, (c) the wheat, (d) the wheat flour and (e) the wheat bran are shown. (f) the pellet form of the C qdots used in the X-ray Diffraction (XRD) measurements are demonstrated. Colloidal C qdots inside 30 ml methanol solution formed at the end of 100 min of ultrasonication are given under (g) a white light and (h) a UV light exposure. (i) C qdots on the Au contact formed by sputtering on a glass slide used in the *IV* measurements.

To understand how exposure time of ultrasonication affected the size and morphology of the formed material, the SEM technique was practised first. The SEM analyses of the samples are given in Figure 2 (a), (b) and (c) respectively. The wheat flour used as purchased was observed to contain microparticles whose mean sizes were found to be 27.1 ± 16.5 μm. These C microparticles were embedded inside larger clusters greater than 100 μm in general and they seem to be randomly distributed throughout the flour sample. The size

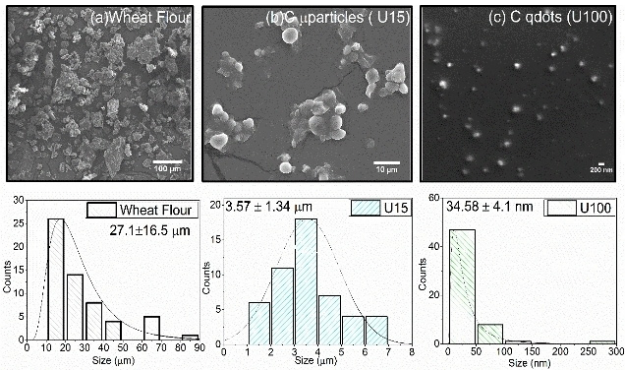

Figure 2. SEM analysis The SEM micrographs of (a) wheat flour (unprocessed), (b) C μparticles and (c) C qdots formed respectively after 15 min and 100 min of ultrasonication at 50 kHz. Their corresponding size distributions (SDs) are given below the each SEM micrograph. The SDs of the wheat flour, U15 and that of U100 seem to fit log-normal, normal and log-normal distributions respectively. The corresponding sizes of the wheat flour, U15 and U100 are 27.1 ± 16.5 μm, 3.57 μm ± 1.34 μm and 34.58 ± 4.10 nm respectively. The SDs found here are shown for the purpose of that the size could be controlled and the C qdots was further investigated using High-resolution Transmission Electron Microscopy (HR-TEM) studies.

and shape of the wheat flour are consistent with those obtained by ultragrinding methods such as the jet milling method.[29] At the end of 15 min and 100 min of the ultrasonication process, U15 and U100 were formed. The surface morphologies of these C materials in the microparticulate and the nanoparticulate forms were found to be almost spherical. In Figure 1 (g) and (h), the C nanoparticles were shown respectively under white and UV light to form a colloidal solution in a common organic solvent such as methanol Energy Dispersive X-ray Spectroscopy (EDS) measurements of the as-prepared C qdots and those exposed to the atmosphere obtained from the reference flour sample are shown in Table 1.

Table 1. The EDS analysis of C qdots formed from wheat flour and that of the flour.

Element [a]	Atomic % (Before)	Atomic % (after) U100 fresh * (2 min)	Atomic % (after) U100 2 hours later *
C K	61.22	84.72	77.28
O K	38.74	10.02	15.74
P K	0.04	-	-
N K	-	5.27	6.97

[a] Here, surface sensitive EDS measurements has been performed from the 1*1 μm^2 area.

The results show that C content was increased after the C qdots were formed. Upon exposing the sample to the atmosphere, the EDS analysis shows a rise on oxides and nitrogen contents. This observation could be explained by several possibilities including C≡N bond or C-N_2O. The Fourier-transform Infrared Spectroscopy (FTIR) measurement was subsequently performed for the as-prepared and the exposed

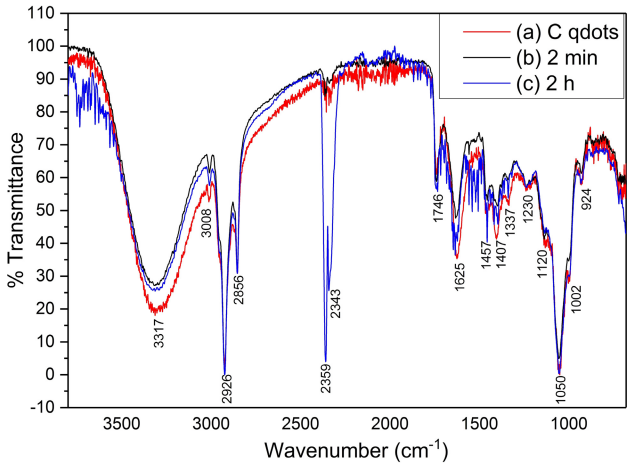

Figure 3. Vibrational spectroscopy results. (a) FTIR measurements of as-prepared C qdots and (b), (c) those exposed to ambient atmosphere 2 min and 2 h respectively where T = 25 °C, P = 1 atm, humidity level: %60. As-prepared C qdots and those exposed to 2 min seem to be associated with *d-glucose*-like traces only and the 2 h exposed sample become associated with a cyano group (C≡N) in addition to *d-glucose*-like traces.

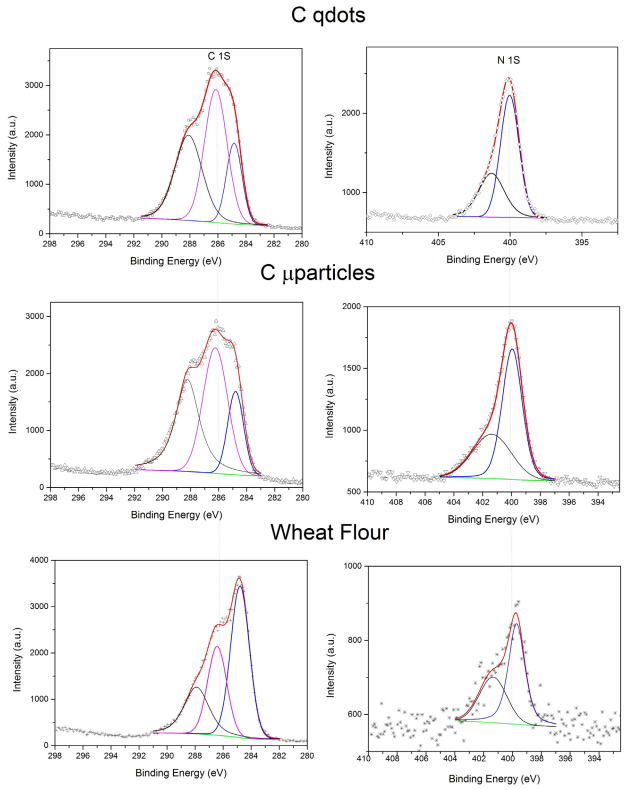

Figure 4. The XPS studies of samples: C qdots, C μparticles and wheat flour. C 1s and N 1s peaks for each sample and their cumulative fits are represented together with the influence from each peak.

samples and the results are shown in Figure 3. It suggests that the as-prepared C qdots can contain d-glucose-like traces. Once exposing the C qdots to the ambient atmosphere for 2 min and 2 hours, the respective FTIR results are given in Figure 3(b) and (c). Here, it is observed that there is an abrupt increase at *ca.* 2359 cm^{-1} at the end of 2 h. Therefore, the EDS results are supported by the FTIR measurements in Figure 1(c) in a way that C≡N bond seems to be formed for the exposed samples.

For overall elemental composition, X-ray Photoelectron Spectroscopy (XPS) measurements were conducted for all samples within an area of 400 μm spot size. The peak table for each sample is shown in Table 2. The XPS studies confirm the

Table 2. The atomic percentages obtained using XPS studies.

Element [a]	Atomic % (Before)	Atomic % (after) U15 exposed	U100 exposed
C K	77.24	66.4	64.52
O K	18.52	22.31	21.74
N K	4.24	11.29	13.74

nitrogen catching capability which was advanced when reducing the size further as shown in the case of the C qdots (U100 sample). For C 1s peak, there are three major peaks appeared at 284.8 ± 0.2 eV, 286 ± 0.2 eV, 288 ± 0.2 eV. These three peaks are assigned respectively to C–C, C–N and C:O groups.[30–32] XPS peak at 286 eV is due to the C–N/C–O bondings.[33,34] Thus, the first deconvoluted peak at 284.8 ± 0.2 eV appears to be due to sp^2 type carbon. The other two peaks at higher energies are considered to be resulted due to bonds between nitrogen and oxygen. The N 1s spectrum in Figure 4 gives peaks at 399.9 ± 0.2 eV and 401.2 ± 0.2 eV, which are assigned for C–N, C=N, CN (nitrile) and N–H species.[30–32,35] FTIR peaks at *ca.* 2359 cm^{-1} and at ca. 3317 cm^{-1} show respectively association with C≡N and N–H bands. Thus, the results demonstrate the presence of amino groups at the surface of the C qdots.

As a preceding investigation technique, the structure and the size of the C qdots powder were determined using powder XRD (p-XRD). Figure 5(a) and Figure 5(b) show respectively the experimental XRD data of the C qdots exposed to the atmosphere and the structural model obtained at the end of the Rietveld analysis. After initial use of a reference pattern (COD ID = 2217266) found in the literature, the Rietveld refinement were completed with a very good quality of fitting (reduced $\chi^2 \approx 1.223$) which suggests that the crystal structure of the C rich qdots was determined to be an acentric primitive orthorhombic structure with a space group of $P2_12_12_1$. The Rietveld analysis also promotes that C rich qdots could catch N atoms and form a stable C≡N bonds the unit cell (see Table S1 and Table S2 for the crystal data and the fractional atomic coordinates respectively). This result was also supported by the FTIR results upon exposing the sample to the atmosphere. In Figure 5(c), how the supramolecules forming the C rich qdots are shown as one asymmetric molecule ($C_{22}H_{22}N_2O_{10}$) connect via the interactions of C–H···O and C–H···N hydrogen bonds to another until the surface was terminated by the H atoms. The intermolecular hydrogen bond distances are comparable to

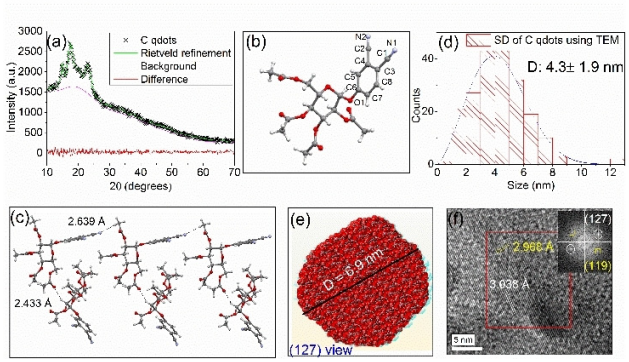

Figure 5. Structural analysis of the C qdots. (a) The experimental XRD data of the U100 sample (black crosses), the fit based on the Rietveld analysis (green line), the background function used (magenta line) and the difference between the XRD data and the fit (red line) are shown. (b) The asymmetric structural unit obtained at the end of the Rietveld refinement of the experimental diffraction pattern and (c) the H bond interactions via O and N atoms are represented to demonstrate the way that the C qdots are formed. C, N, O and H atoms are designated by black, blue, red and white balls. Two examples of the interactions of C–H···O and C–H···N hydrogen bonds are demonstrated and their bond lengths were respectively found to be 2.431 Å and 2.637 Å. (d) The size distribution the C –qdots found using the HR-TEM technique and Weibull distribution curve (blue colour) (e) One illustration of the C qdots in (127) view with a size of 6.9 nm in diameter. (e) HR-TEM image of the C qdots showing the respective lattice planes for (119) and (127). An FFT image was shown in the inset to represent the corresponding diffraction spots taken from the rectangular area (red colour) in the HR-TEM image.

those previously reported[36,37] (see Table S3 for all of the intermolecular hydrogen bonds and their respective lengths). This was also found to be almost consistent with the EDS and the XPS results since an increase in the N contents was observed upon exposing the sample to the atmosphere.

The crystallite size was also determined using the Debye-Scherer law[36] and approximately found to be 5.6 ± 0.6 nm. This might give the impression to be contradicting with the size estimated by the SEM results. However, the SEM measurements might also appear to fail at detection of the smaller nanoparticles and might be limited due to the relatively low sensitivity of the technique. This would make us biased to count larger particles size and ignore those relatively smaller. On the other hand, an immediate exposure of the sample to the more energetic electron beams such as at 30 kV causes an irrecoverable damage on the sample and this makes utilisation of a more sensitive electron probe technique including a TEM measurement (working at energies ≥100 keV) hard. Still, we have attempted to use the HR-TEM and the effect of the high energy electron beam was observed to be dominant particularly for larger clusters whose size is larger than 100 nm. Such clusters seemed to be formed due to agglomeration on the grid. However, for isolated smaller nanoparticles, the beam effect was not observed. Figure 5(d) shows the size distribution of the C qdots obtained using 200 qdots (see Figure S1). From this data, the mean size of the C qdots was found to be 4.3.± 1.9 nm in diameter which is consistent with the size found using the XRD data. The HR-TEM image in Figure 5(e) represents the lattice fringes corresponding to (119) and (127) planes as an indicator of to the orthorhombic structure proposed by the Rietveld analysis.

Optical Properties of C qdots

For the optical properties, the photoluminescence (PL) measurements of C qdots (U100) with the excitation wavelengths of 405 nm, 488 nm, 532 nm and 635 nm are shown in Figure 6 (a),

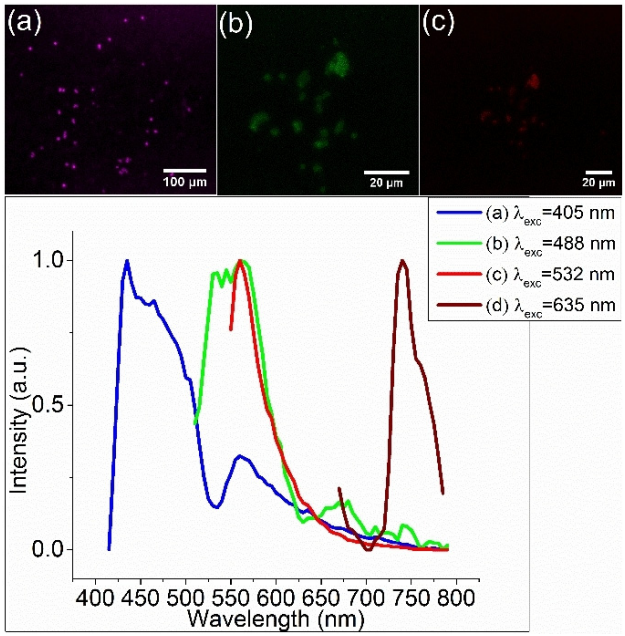

Figure 6. Wavelength-dependent light emission properties of C qdots. LSCM images and corresponding photoluminescence results are given for the excitation wavelengths of 405 nm, 488 nm, 532 nm and 635 nm. The LSCM image for the excitation wavelength of 635 nm is not shown since the fluorescent image was not obtained. Corresponding photoluminescence spectra show the red shift in the emission of C qdots.

(b), (c) and (d) respectively. The excitation dependent red shift is well-known characteristics of organic C qdots prepared from green sources.[13,17,20] The source of luminescence of the C qdots may stem from nanoparticle size as well as from surface defects. In addition, the existence of different functional groups on the surface can cause a shift in the absorbance which in return results in a shift in the PL emission.[19]

Decreasing the size from microscale to nanoscale shows enhancement of the PL intensity in Figure 7(a) and (b) respectively for the colloidally stable C qdots. We can infer the possible electronic transitions for the results given in Figure 6 and Figure 7 by revisiting the absorption of light by the polyatomic molecules in organic samples.[37] C bonds in a C qdot include σ and π bonds. Thus, once exciting the C qdots as in the case of a PL measurement depending on the excitation wavelength, σ→σ*, σ→π*, π→π* and n→π* transitions could be considered to arise. The absorption data of the C qdots (U100) in Figure 7 shows that π→π* transitions occur due to species such as carbonyl groups conjugated to the benzene

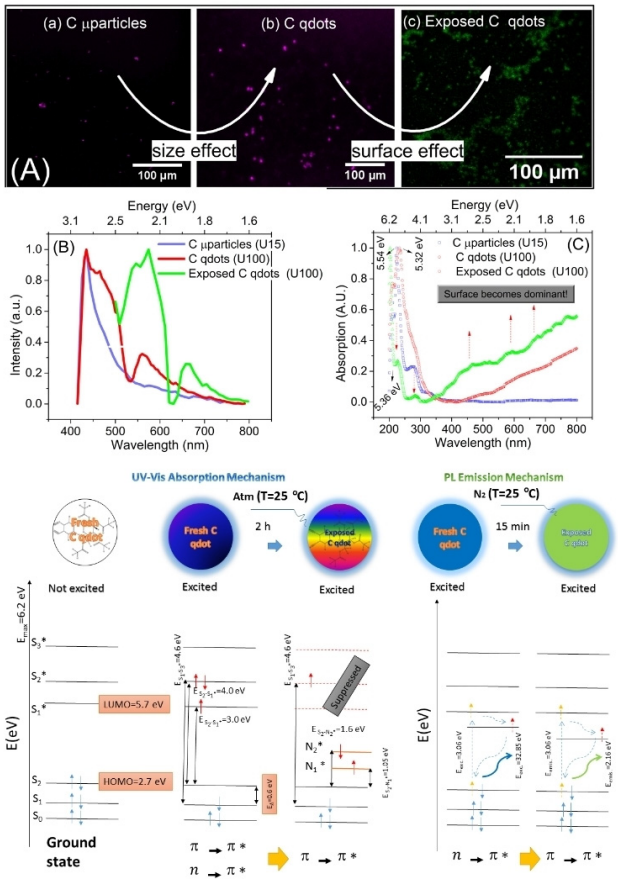

Figure 7. Size and surface effects on the light emission properties of C qdots. (A) LSCM images of (a) U15, (b) as-prepared U100 sample and (c) the N_2 exposed U100 sample, (B) corresponding photoluminescence results at the excitation wavelength of 405 nm and (C) the UV-Vis absorption spectroscopy data are shown. The possible mechanisms are schematically demonstrated. The size effect shows an intensification in the PL emission due to increase in the number of n→π* transitions. The surface states were formed due to N atoms caught by C molecules in the C qdot surface which in return would result in the red shift in the PL emission attributed to the transformation from n→π* transition to π→π*transition.

ring at 233 nm (*ca.* 5.32 eV) and that the σ orbital electrons was not excited since such σ→σ* transitions require much higher energies usually in far UV region. On the other hand, π orbitals do no overlap with σ orbitals, therefore, π→π* transitions are independent of each other. Figure 7(B) shows a red shift in the PL emission which is considered to be due to the surface of the C qdots adsorbed O or N after exposing the sample to the ambient atmosphere (see Table 2). Figure 3 shows there is an abrupt change due to the formation of nitrile bonds located *ca.* 2359 cm^{-1}. On the other hand, the absorption data of the exposed C qdots given in Figure 7(C) shows the absorption band due to the carbonyl bonds was shifted to *ca.* 227 nm (5.46 eV) and suppressed with respect to that in the as-prepared C qdots. Nevertheless, the absorption from the visible to the beginning of the NIR region (400-800 nm) seemed to be relatively intensified for the exposed sample. To understand the vulnerability of the sample against only N_2 gas in the atmosphere, we left the as-prepared sample in the N_2 gas medium for 15 min at room temperature. There is a minor change in the corresponding FTIR spectrum compared to that of the as-prepared sample (see Figure S2). Nonetheless, as shown in Figure 7(B), there is an obvious bathochromic shift in the PL emission of the exposed C qdots. These results suggest that the light emission appear to be red-shifted due to the formation of new species particularly C≡N bonds. Thus, these results suggest the formation of the surface states active in the light emission and a transformation from the n→π* transitions to the π→π* transitions when the as-prepared sample was removed from methanol and exposed to the ambient atmosphere where nitrogen is present. Furthermore, the optical band gap calculations of the C qdots were done using the absorption data given in Figure 7 by Tauc's model.[38] These results are also tabulated in Table 3 for the direct and indirect transitions of the

Table 3. The HOMO to the LUMO energy levels determined using Tauc's relation for the direct and the indirect transitions.

Transitions	The as-prepared C qdots		The exposed C qdots	
	Direct	Indirect	Direct	Indirect
S_1-S_2*	3.0	2.95	-	-
S_2-S_2*	3.6	3.1	-	-
S_2-S_1*	4.6	3.3	4.6	-
S_2-S_3*	-	4.1	-	3.7
S_2-N_1*	-	-	1.05	0.2
S_2-N_2*	-	-	1.6	-

as-prepared C qdots and the exposed C qdots. Three energy levels from the highest occupied molecular orbital (HOMO) to the **lowest** unoccupied molecular orbital (LUMO) were determined to be present for the direct transitions of the fresh C qdots. For the direct band gap calculations of the as-prepared C qdots, the transitions were determined to be 3.0 eV, 4.0 eV, 4.6 eV from S_1-S_2*, S_2-S_2* and S_2-S_1* levels respectively. The valance band was obtained using the XPS measurements and found to be *ca.* 2.7 eV. As a result, the conduction band position (LUMO) for the as-prepared C qdots could be found to be 5.7 eV for the direct transitions. The surface states were observed to be intensified and the previous transitions relatively became suppressed upon exposing the C qdots to the ambient atmosphere. The corresponding surface state energy levels were similarly found using Tauc's relation for the direct and the indirect transitions of the exposed C qdots. These energy levels were determined to be 1.05 eV and 1.6 eV respectively for the S_2-N_1* and the S_2-N_2* transitions. The surface states were observed to be intensified and the previous transitions relatively became suppressed upon exposing the C qdots to the ambient atmosphere. The corresponding surface state energy levels were similarly found using Tauc's relation for the direct and the indirect transitions of the exposed C qdots. These energy levels were determined to be 1.05 eV and 1.6 eV respectively for the S_2-N_1* and the S_2-N_2* transitions.

Electrical Properties and Electrocatalytical Performance of C qdots

We then investigated I–V characteristics of the exposed U100 sample under various temperatures from 25 °C to 250 °C with 5 °C increments. In Figure 8(a), we represent the initial portion of

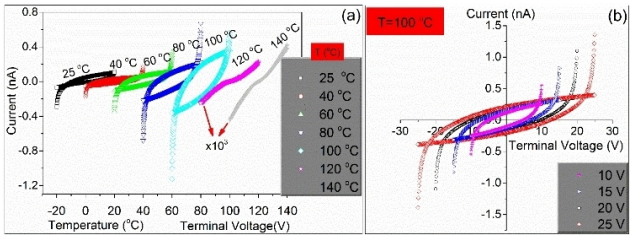

Figure 8. I–V characteristics of the C qdots. (a) Temperature dependent I–V measurements of the U100 sample are shown from 25 °C to 140 °C. Here, the terminal voltage was applied from −20 V to 20 V and vice versa for each temperature point. For clarity, the graphs in the horizontal axis (terminal voltage) was shifted and the current values for the temperatures of 120 °C and 140 °C were minified 1000 times. (b) The I–V characteristics at different terminal voltages from 10 V to 25 V are shown for the temperature of 100 °C.

the electrical measurements from 25 °C to 120 °C. The I–V characteristics at 25 °C show a loop when applying a positive and negative bias (from −20 V to +20 V and vice versa respectively). Nevertheless, the question might arise[27] whether this behaviour is a relaxor ferroelectric behaviour as reported by Cross[39] and Hemberger *et al.*[26] or just a typical lossy dielectric behaviour pointed by Scott.[28] Scott indeed showed a real banana skin demonstrates such cigar-like shapes in his *Polarization-Electric Field* (*P-E*) measurement. Nevertheless, we did not stop and collected the data to see such loops would end and show a paraelectric behaviour at elevated temperatures like traditional ferroelectrics. This loop continues with an increase in the remanant current till 120 °C where it shows paraelectric-like behaviour.

The nature of the asymmetric molecule and the charge-separation due to the intermolecular hydrogen bonds (Figure 5(b) and (c) respectively) are considered to cause a permanent dipole present throughout the corresponding monolayer and finally a net dipole in the C qdots. On the other hand, comparing with some examples of the typical ferroelectric materials such as $PbZr_XTi_{1-X}O_3$ (PZT),[40] $SrBi_2Ta_2O_9$ (SBT),[41] and $(Bi,La)_4Ti_3O_{12}$ (BLT),[42] their characteristics after a transition from the ferroelectric phase to the paraelectric phase when reaching the transition temperature could be considered to be closely akin to that of the U100 sample. In addition, applying different terminal voltages including 10 V, 15 V, 20 V and 25 V similarly shows such bipolar characteristics as given in Figure 7(b). This behaviour is reversible when cooling from 120 °C to room temperature (RT). However, heating the sample until 250 °C preserves the paraelectric like phase even it is cooled down to the RT.

We further tested C qdots (the U100 sample) in oxygen reduction reaction (ORR) since nitrogen-doped carbon is a well-known catalyst for the noble metal free ORR catalysis. The EDS data, the FTIR results, the XPS results and the predicted structure from the XRD data clearly show the presence of nitrogen in the C qdots thus its ORR catalytic activity is screened in the alkaline solution. CVs were obtained at the CNT/GC, C qdots-CNT/GC and PtC/GC under N_2 and O_2 saturated KOH solution. Figure 9(a) shows CV at the C qdots-

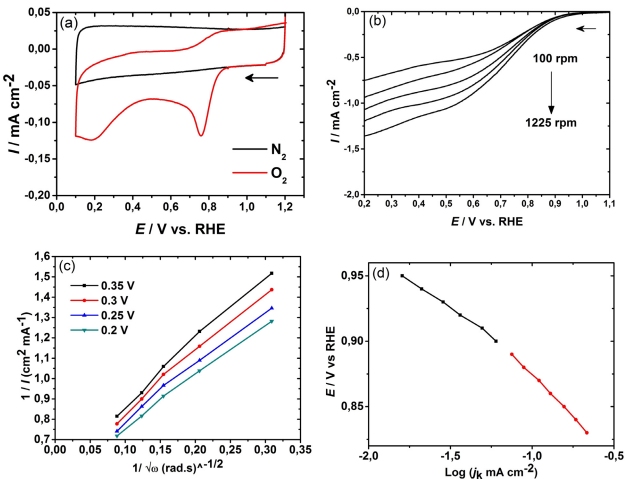

Figure 9. ORR activity of C qdots (U100 sample) (a) CV obtained at C qdots-CNT/GC under saturated N_2 and O_2 0.1 M KOH, at 50 mV/s *vs.* RHE. (b) Linear sweep voltammetry of C qdots-CNT/GC at different rotation 100–1225 rpm under saturated O_2 0.1 M KOH, at 10 mV/s *vs.* RHE. (c) and (d) show the Koutecky–Levich plot and Tafel plot, respectively (Data used from 8(b)).

CNT/GC (The data obtained at the CNT/GC and PtC/GC can be found in Figure S3 and S4 respectively in the SI). The onset potentials for ORR at the CNT/GC, C qdots -CNT/GC and PtC/GC were 0.8, 0.9 and 0.98 V vs. RHE, respectively which clearly indicates that the addition of C qdots catalyses the ORR process more efficiently than the bare CNT. In these measurements more anodic onset potential implies better ORR catalytic activity. Although the onset potential of C qdots-CNT/GC is 80 mV cathodic than the standard PtC catalyst, C qdots are drastically cheaper than Pt catalyst and the easy and green synthesis of C qdots can reduce the cost of energy devices and enable simple scale up for the commercialization.

To realize ORR mechanism and kinetics, rotating disc electrode (RDE) measurements were carried out (Figure 9(b)). The numbers of electrons involved in the ORR and Tafel slope were estimated using this data and summarized in Table 4 (Detail calculation process is described in the Supporting Information (SI)). Based on the number electrons involved in the ORR at the C qdots-CNT/GC from Figure 9(c), two pathways of ORR mechanism can be predicted i.e. parallel ($k_1 = k_2$ and $k_3 = 0$) and serial ($k_2 = 2 \times k_3$ and $k_1 = 0$) pathways shown in (Scheme S1).[43] However, these parameters estimated for the CNT/GC demonstrate that the ORR follows the serial pathway ($k_2 = k_3$ and $k_1 = 0$) favourably with ca. 2 electron process. Thus, in case of C qdots-CNT/GC, ORR at C qdots and uncovered CNT surfaces cannot be ruled out with the number of electrons 4

Table 4. The numbers of electrons involved in the ORR and Tafel slop at the C qdots-CNT/GC, CNT/GC and PtC/GC under N_2 and O_2 saturated KOH solutions.

Electrode	Onset potentia /V vs. RHE	No. of electrons	Tafel slope HCD/ LCD mV/dec	$E_{1/2}$ at 400 rpm/ mV
C qdots-CNT/GC	0.9	3	129/85	730
CNT/GC	0.8	2.0	185/96	620
PtC/GC	0.96	3.9	119/59	850

and 2 respectively, which can cumulatively result as 3. The electrocatalytic ORR process is efficient at C qdots-CNT/GC than the reported study at nitrogen-doped C qdots which showed 2 electron ORR. However, hydrothermally deposited nitrogen-doped C qdots on the graphene[44] and graphene oxide[45] show 4 electron ORR. Thus, present study further proves the importance of the carbon material used as a support for the C qdots and influence of method used to attach C qdots on the supportive carbon materials towards ORR process.

The change of adsorbed reaction intermediates from Temkin to Langmurian conditions or the changing concentration of OH on the surface, influences the adsorption of O_2 molecules and this leads to the two Tafel slopes at low current density (LCD) and high current density (HCD) regions. In Figure 9(d), the 129/85 Tafel slop for HCD/LCD at the C qdots-CNT/GC reflects that first step is the rate liming process in the ORR. Furthermore, the Tafel slope of the C qdots-CNT/GC is lower than the CNT/GC. Thus, lower Tafel slope at the C qdots-CNT/GC than the CNT-GC and higher kinetic current density $E_{1/2}$ at clearly proves that C qdots are catalytically more efficient than CNT.

Conclusions

In summary, our results show that the luminescent C qdots could be formed with various sizes by a facile green synthesis method. The temperature dependent I–V characteristics of the C qdots suggest showing a relaxor ferroelectric behaviour. Another important aspect of this study is that the C qdots could catch N atoms in addition to an increase in the O content upon exposing the sample to the atmosphere. Besides, our N-doped C qdots were demonstrated to show a good performance for ORR activity carrying the potential for formation of cost-effective fuel cells and batteries. The C qdot sample due to its N content (≈7%) seems to be passing to decomposing limit (sufficient N content = % 1.7 for decomposing of the rye plants[46]) when placing the sample in the soil. Therefore, this study can open a new age for the synthesis of the organic electronic devices which can be decomposing naturally upon leaving the sample into the soil.

Supporting Information Summary

Supporting information is provided including the experimental section, HR-TEM images, FTIR spectrum of the N_2 exposed C qdot, table of the crystal data and structural parameters, and table of fractional atomic coordinates and isotropic or equivalent isotropic displacement parameters and table of intermolecular hydrogen bonds and their lengths. The calculations for ORR and electrochemical data for CNT/GC and PtC/GC are also provided in the SI. For crystallographic data of the 100 sample, see cif deposited the Cambridge Crystallographic Data Centre with deposition number of CCDC 1511040.

Acknowledgements

We would like to acknowledge the support provided by Electrical and Electronics Engineering at Istanbul Arel University (IAU) and UNAM at Bilkent University in Turkey. The project was supervised by A.K at the Institute of Science and Technology, IAU.

Conflict of Interest

The authors declare no conflict of interest.

Keywords: Carbon · catalytic activity · ferroelectric · organic · quantum dots

[1] S. Iijima, *Nature* **1991**, *354*, 56–58.
[2] M.-F. Yu, B. S. Files, S. Arepalli, R. S. Ruoff, *Phys. Rev. Lett.* **2000**, *84*, 5552–5555.
[3] K. S. Novoselov, A. K. Geim, S. V. Morozov, D. Jiang, Y. Zhang, S. V. Dubonos, I. V. Grigorieva, A. A. Firsov, *Science (80-.).* **2004**, *306*, 666–669.
[4] M. P. Levendorf, C.-J. Kim, L. Brown, P. Y. Huang, R. W. Havener, D. a. Muller, J. Park, *Nature* **2012**, *488*, 627–632.
[5] E. Petryayeva, W. R. Algar, I. L. Medintz, *Appl. Spectrosc.* **2013**, *67*, 215–252.
[6] J. Li, J.-J. Zhu, *Analyst* **2013**, *138*, 2506–15.
[7] T. Xing, J. Sunarso, W. Yang, Y. Yin, A. M. Glushenkov, L. H. Li, P. C. Howlett, Y. Chen, *Nanoscale* **2013**, *5*, 7970.
[8] G. Panomsuwan, N. Saito, T. Ishizaki, *Phys. Chem. Chem. Phys.* **2015**, *17*, 6227–6232.
[9] H. K. Sadhanala, R. Nandan, K. K. Nanda, *Green Chem.* **2016**, *18*, 2115–2121.
[10] R. Hardman, *Environ. Health Perspect.* **2006**, *114*, 165–172.
[11] N. Singh, B. Manshian, G. J. S. Jenkins, S. M. Griffiths, P. M. Williams, T. G. G. Maffeis, C. J. Wright, S. H. Doak, *Biomaterials* **2009**, *30*, 3891–914.
[12] V. L. Colvin, *Nat. Biotechnol.* **2003**, *21*, 1166–70.
[13] A. B. Bourlinos, A. Stassinopoulos, D. Anglos, R. Zboril, M. Karakassides, E. P. Giannelis, *Small* **2008**, *4*, 455–458.
[14] H. Li, X. He, Y. Liu, H. Yu, Z. Kang, S. T. Lee, *Mater. Res. Bull.* **2011**, *46*, 147–151.
[15] X. He, H. Li, Y. Liu, H. Huang, Z. Kang, S. T. Lee, *Colloids Surfaces B Biointerfaces* **2011**, *87*, 326–332.
[16] J. Wang, C. F. Wang, S. Chen, *Angew. Chemie - Int. Ed.* **2012**, *51*, 9297–9301.
[17] S. Sahu, B. Behera, T. K. Maiti, S. Mohapatra, *Chem. Commun.* **2012**, *48*, 8835.
[18] A. Khanam, S. K. Tripathi, D. Roy, M. Nasim, *Colloids Surfaces B Biointerfaces* **2013**, *102*, 63–69.
[19] B. De, N. Karak, *RSC Adv.* **2013**, *3*, 8286.
[20] D. Chowdhury, N. Gogoi, G. Majumdar, *RSC Adv.* **2012**, *1*, 12156–12159.
[21] M. P. Sk, A. Jaiswal, A. Paul, S. S. Ghosh, A. Chattopadhyay, *Sci. Rep.* **2012**, *2*, 1–5.

[22] A. Abbassian, J. Pound, Food Outlook BIANNUAL REPORT ON GLOBAL FOOD MARKETS: Wheat, **2016**.
[23] National Nutrient Database for Standard Reference Release 28, *Statistics Report: 20649, Wheat Flour, Whole-Grain, Soft Wheat*, **2016**.
[24] P. Weaver, M. G. Cain, in *Characterisation Ferroelectr. Bulk Mater. Thin Film.*, **2014**, pp. 115–145.
[25] N. Choudhury, L. Walizer, S. Lisenkov, L. Bellaiche, *Nature* **2011**, *470*, 513–517.
[26] J. Hemberger, P. Lunkenheimer, R. Fichtl, H.-a. Krug von Nidda, V. Tsurkan, A. Loidl, *Nature* **2005**, *434*, 364–367.
[27] J. Hemberger, *Nature* **2007**, *448*, E4–E5.
[28] J. F. Scott, *J. Phys. Condens. Matter* **2007**, *20*, 21001.
[29] S. Protonotariou, I. Mandala, C. M. Rosell, *Food Bioprocess Technol.* **2015**, *8*, 1319–1329.
[30] Y. Zhang, Y. H. He, P. P. Cui, X. T. Feng, L. Chen, Y. Z. Yang, X. G. Liu, *RSC Adv.* **2015**, *5*, 40393–40401.
[31] Q. Niu, K. Gao, Z. Lin, W. Wu, *Anal. Methods* **2013**, *5*, 6228.
[32] R. Zhang, W. Chen, *Biosens. Bioelectron.* **2013**, *55*, 83–90.
[33] M. Rong, Y. Feng, Y. Wang, X. Chen, *Sensors Actuators, B Chem.* **2017**, *245*, 868–874.
[34] X. Wang, J. Cheng, H. Yu, J. Yu, *Dalt. Trans.* **2017**, *46*, 6417–6424.
[35] A. Mueller, M. G. Schwab, N. Encinas, D. Vollmer, H. Sachdev, K. Müllen, *Carbon N. Y.* **2015**, *84*, 426–433.
[36] R. K. Agrawalla, *Express Polym. Lett.* **2016**, *10*, 780–787.
[37] B. Valeur, in *Mol. Fluoresc. Princ. Appl.*, Wiley-VCH Verlag, **2001**, p. 20.
[38] J. Tauc, R. Grigorovici, A. Vancu, *Phys. status solidi* **1966**, *15*, 627–637.
[39] L. E. Cross, in *Piezoelectricity*, Springer Berlin Heidelberg, Berlin, Heidelberg, **2008**, pp. 131–155.
[40] P. K. Panda, B. Sahoo, *Ferroelectrics* **2015**, *474*, 128–143.
[41] T. J. Boyle, C. D. Buchheit, M. A. Rodriguez, H. N. Al-Shareef, B. A. Hernandez, B. Scott, J. W. Ziller, *J. Mater. Res.* **1996**, *11*, 2274–2281.
[42] H. Nakayama, O. Sugiyama, T. Mano, Y. Shibuya, Y. Hoshi, H. Suzuki, *Jpn. J. Appl. Phys.* **2005**, *44*, 6947–6951.
[43] R. Mishra, B. Patil, F. Karadaş, E. Yılmaz, *ChemistrySelect* **2017**, *2*, 8296–8300.
[44] C. Hu, C. Yu, M. Li, X. Wang, Q. Dong, G. Wang, J. Qiu, *Chem. Commun.* **2015**, *51*, 3419–3422.
[45] W. J. Niu, R. H. Zhu, Yan-Hua, H. B. Zeng, S. Cosnier, X. J. Zhang, D. Shan, *Carbon N. Y.* **2016**, *109*, 402–410.
[46] S. A. Waksman, F. G. Tenney, *Soil Sci.* **1927**, *24*, 317–333.

Submitted: March 9, 2018
Revised: April 9, 2018
Accepted: April 10, 2018